High Voltage Studies of Inverted-geometry Ceramic Insulators for a 350 kV DC Polarized Electron Gun

C. Hernandez-Garcia, M. Poelker, and **J. Hansknecht**
Thomas Jefferson National Accelerator Facility
12000 Jefferson Ave
Newport News, VA 23606, USA

ABSTRACT

Jefferson Lab is constructing a 350 kV direct current high voltage photoemission gun employing a compact inverted-geometry insulator. This photogun will produce polarized electron beams at an injector test facility intended for low energy nuclear physics experiments, and to assist the development of new technology for the Continuous Electron Beam Accelerator Facility. A photogun operating at 350kV bias voltage reduces the complexity of the injector design, by eliminating the need for a graded-beta radio frequency "capture" section employed to boost lower voltage beams to relativistic speed. However, reliable photogun operation at 350 kV necessitates solving serious high voltage problems related to breakdown and field emission. This study focuses on developing effective methods to avoid breakdown at the interface between the insulator and the commercial high voltage cable that connects the photogun to the high voltage power supply. Three types of inverted insulators were tested, in combination with two electrode configurations. Our results indicate that tailoring the conductivity of the insulator material, and/or adding a cathode triple-junction screening electrode, effectively serves to increase the hold-off voltage from 300kV to more than 375kV. Electrostatic field maps suggest these configurations serve to produce a more uniform potential gradient across the insulator.

Index Terms — **Electron guns, high-voltage techniques, insulators, vacuum insulation.**

1 INTRODUCTION

MANY high-energy and nuclear physics experiments are conducted using spin-polarized electron beams produced by illuminating a GaAs photocathode inside a direct current (dc) high voltage photogun with circularly polarized light [1]. The vacuum conditions within the photogun must be below 10^{-9} Pa to maintain a reasonable photocathode operating lifetime [2]. At most facilities worldwide, the photocathode is biased at 100 kV. Higher bias voltages would serve to improve beam quality, but historically, attempts to operate dc high voltage polarized photoguns above 100 kV have proven very difficult, primarily due to field emission that degrades vacuum conditions. Radio frequency (RF) electron guns produce beams at much higher energy (in the Mega electron-Volt range) but their operating vacuum conditions preclude the use of GaAs photocathodes [3]. Recent worldwide interest in developing bright accelerator-based light sources has renewed efforts to operate dc high voltage photoguns at considerably higher voltages (500 kV or more). At Jefferson Lab, an inverted-geometry ceramic insulator approach has been adopted, where the term "inverted" describes an insulator that extends into the vacuum chamber serving as the cathode electrode support structure [4]. This represents an alternative to designs that employ large cylindrical insulators with long metal electrode support tubes passing through the insulator bore [5-7]. The inverted-insulator design helps to reduce field emission because there is considerably less metal biased at high voltage. However, the inverted-geometry ceramic insulator introduces a new problem compared to other photogun designs, namely, how to effectively apply high voltage to the cathode electrode without encountering high voltage breakdown across the relatively small inverted insulator.

The first photogun to employ an inverted insulator design was developed at the Stanford Linear Accelerator Center (SLAC) with reported operating voltage of 120 kV [8]. The SLAC design relied on three hollow cylindrical insulators: two served to provide cathode cooling and one as a conduit to apply the high voltage. Another spin-polarized electron source with an inverted-insulator design was implemented for the Bonn Electron Stretcher Accelerator, ELSA, albeit operating at just 50 kV [9]. The Jefferson Lab inverted-insulator design employs one conical-shaped insulator that

Manuscript received on 3 December 2014, in final form 28 August 2015, accepted 1 September 2015, accepted 31 August 2015.

DOI 10.1109/TDEI.2015.005126

extends into the vacuum chamber. The insulator is a common component of medical x-ray devices, with the commercial designation "R28", which specifies the length and angle of the interior conical shape. Because these insulators are widely used, they are relatively inexpensive, and they mate to commercial high voltage cables. Two photoguns have been constructed at Jefferson Lab using the R28 insulator: one provides spin-polarized electron beams for the Continuous Electron Beam Accelerator Facility (CEBAF) at 130 kV bias voltage, and the other is used at a test facility to produce beam at 200 kV and at beam currents up to 4 mA dc [10]. The objective of this work was to develop an inverted-ceramic/electrode geometry capable of reaching 375 kV, without electrical breakdown for nominal operation at 350 kV. At 350 kV bias voltage, the extracted electron beam is sufficiently relativistic (traveling at 0.8 c) to accommodate beam injection directly into a standard CEBAF superconducting RF accelerating module, without pre-acceleration using a graded-beta RF "capture" cavity, thereby significantly reducing the cost and complexity of the injector design.

Three types of inverted insulators were tested: unaltered alumina, vendor-proprietary doped alumina that provides a small level of bulk conductivity, and alumina coated with zirconium oxide (ZrO) intended to provide a small level of surface conductivity. Most tests were performed using insulators with the R30 designation, which are longer than R28 insulators. In addition, one of the unaltered alumina insulators was evaluated using a screening electrode near the cathode-vacuum-insulator triple junction. All tests were conducted using a spherical stainless steel test electrode that was mechanically polished to mirror-like finish to minimize field emission. The test electrode did not accommodate a photocathode. All tests employed commercial high voltage cables connected to a Cockcroft-Walton 580 kV dc high voltage power supply within a pressure vessel that was filled with sulfur hexafluoride (SF_6) at 69 kPa (10 pounds per square inch). Results from two of the four test configurations show that the electrode can be biased to higher voltages without breakdown at the insulator/cable interface. We offer possible explanations for why these two configurations performed better than the others.

2 EXPERIMENTAL SETUP AND PROCEDURES

High voltage tests conducted with electrodes inside vacuum chambers often lead to field emission, which produces x-rays. As such, all measurements were conducted using equipment within a concrete-shielded room and via remote control. Access to the room was prohibited when the high voltage power supply was energized, using interlocks that were part of an engineered personnel safety system.

2.1 APARATUS

The photogun high voltage test chamber is cylindrical (46 cm diameter) with a flat-front plate and dish-head back plate, made of 304 stainless steel (Figure 1a). The inverted insulators were welded to custom 25.4 cm diameter stainless steel Conflat vacuum flanges. The chamber was previously vacuum baked at 400 °C for 100 hours to reduce outgassing from the chamber walls [11]. Vacuum pumping was provided using a small ion pump and a non-evaporable getter (NEG) pump module positioned where the anode electrode would normally reside, when the photogun is eventually configured to provide an electron beam. Prior to each high voltage test, the chamber was evacuated using a turbo pump and the entire system baked within an oven at 250 °C for 48 hours. The bakeout served to eliminate water vapor from the vacuum apparatus and to partially activate the NEG module. Vacuum in the low 10^{-9} Pa was routinely achieved and a residual gas analyzer (200 atomic mass unit resolution) was used to verify the system was free of vacuum leaks.

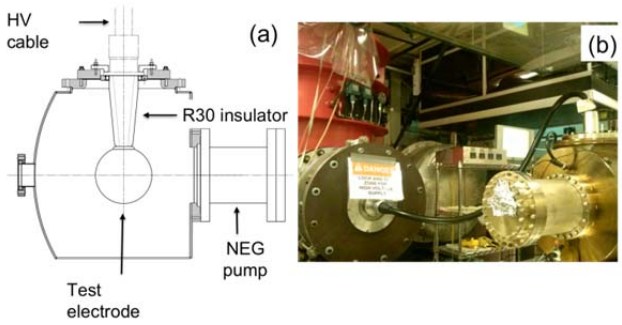

Figure 1. Schematic representation of the photogun high voltage vacuum chamber showing the test electrode (15.25 cm diameter) supported by an R30 inverted insulator (a) and photograph of the high voltage test chamber connected to the power supply via a commercial high voltage cable (b). The high voltage power supply resides within the red-colored SF_6 tank.

As mentioned above, most tests were conducted using the R30 insulators that position the test cathode electrode in the middle of the vacuum chamber as shown in Figure 1a. The test electrode was spherical (15.24 cm diameter), without the means to accept a photocathode. It was manufactured from two hemispheres of hydroformed 304 stainless steel sheet that were welded together and polished by hand using silicon carbide paper to obtain a mirror-like surface finish. Toward the end of the experiment, while waiting for the arrival of a machined component, time was available to polish the test electrode further using diamond grit. In retrospect, diamond-paste polishing was not required, as field emission was already very low. The anode for these measurements was simply the grounded vacuum chamber wall that provided a minimum cathode/anode gap of approximately 10 cm. For an actual photogun, the cathode electrode would possess additional apertures to accommodate a photocathode that could be inserted or removed from the electrode using a vacuum sample manipulator [10].

Commercial industrial high voltage cables with appropriate R28 or R30 terminations were used to connect the photogun to the high voltage power supply. Cables were typically 4 meters long, with capacitance of 102 pF per meter, providing stored energy of 25 J at 350 kV including the 12 pF capacitance of the photogun. One end of the cable was

connected to an R28 or R30 inverted-insulator at the test chamber, and the other end was connected to the dc high voltage power supply inside the SF_6 pressure vessel, via a molded epoxy receptacle. The epoxy receptacles were also commercial components with R28 and R30 designations. A 300 MΩ conditioning resistor was placed in series between the epoxy receptacle and the high voltage power supply, within the SF_6 vessel, to limit the available current that could be delivered from the high voltage power supply, and to protect the electrode via a negative feedback mechanism – as current increased due to field emission or breakdown, a larger voltage drop occurred across the resistor, thus reducing the voltage at the electrode. However, the placement of the resistor does not protect the insulator/electrode assembly from the stored energy in the high voltage cable.

2.2 MATERIALS AND CONFIGURATIONS

A total of five inverted insulators were tested: three R30 insulators each 20 cm long composed of 97.7% alumina and labeled as 'R30 unaltered alumina'. A fourth R30 unaltered alumina insulator was coated on the vacuum side with a ZrO film to test if reducing the insulator surface resistivity would increase the breakdown voltage by facilitating surface charge drainage [12, 13]. A commercial vendor, Atkinson Thin Film Systems INC, applied the coating by sputtering zirconium from a source attached to a fixed arm in an oxygen-rich environment, with the insulator nearby and rotating. Two source positions were used to obtain a more uniform coating. Preliminary tests with coupons indicated that the resistivity of the coating could be adjusted by varying the sputtering time, and consequently the coating thickness. However we subsequently learned resistance values were not stable, as the coating oxidized in air. The fifth insulator was a shorter R28 version, 13 cm long and composed of 94.4% alumina doped with a proprietary formulation that served to reduce the insulator bulk resistivity. As with the R30 ZrO-coated insulator, the intent was to test if a certain degree of bulk conductivity served to increase the breakdown voltage by providing charge buildup drainage [14-16]. All of the insulators were purchased from Solutions in Ceramic Technologies (SCT-France). Each insulator was delivered with a brazed molybdenum end piece at the narrow end of the taper to provide vacuum isolation as well as mechanical and electrical contact to the electrode at the vacuum side, and to the cable plug on the air side. The outer rim of the insulator, on the wide end of the taper, was brazed to a kovar ring and welded (vacuum tight) to a custom 25.4 cm diameter stainless steel Conflat vacuum flange. Figure 2 shows examples of all types of tested insulators.

Two insulator/electrode configurations were evaluated. The majority of tests were conducted using a mounting cup with a rounded collar manufactured from 304 stainless steel that provided a means to attach the test spherical electrode to the insulator. The mounting cup was affixed to the electrode using four setscrews that protrude from the cup and press against the interior of the spherical shell electrode. The spherical electrode and mounting cup were then screwed onto the molybdenum plug of the insulator using a short threaded rod. The other configuration employed a screening electrode also manufactured from 304 stainless steel intended to linearize the potential gradient across the insulator length. In this configuration, the narrow end of the R30 insulator was recessed into the now larger cathode electrode assembly, resembling configurations tested in [17] that yielded increased voltage holdoff compared to electrodes without screening.

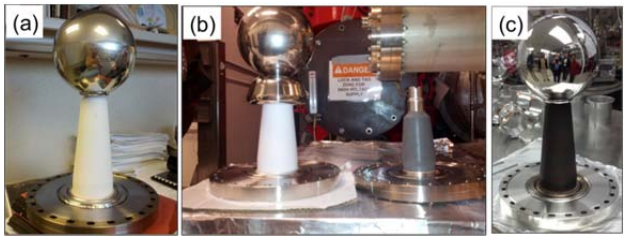

Figure 2. Photographs of insulators and electrode configurations, each shown welded to 25.4 cm diameter stainless steel Conflat vacuum flange. The same spherical electrode (15.25 cm diameter) was used for every test. In (a) the R30 unaltered alumina insulator ~ 20 cm long. In (b) the R30 unaltered alumina insulator with screening electrode covering the triple point junction. For comparison, the shorter R28 doped alumina insulator (~ 13 cm long) was placed nearby, without an electrode attached, and (c) the R30 unaltered alumina insulator with ZrO coating on the vacuum side.

All of the metal components that were biased at high voltage (test electrode, collar, and screening electrode) were polished by hand to provide an exceptionally smooth surface, to minimize field emission. Briefly, the procedure in [18] was as follows: polishing begins with 180 grit paper (i.e., 180 particles per square inch). Two sheets of polishing paper were wet in a solution of coconut oil and de-ionized water and rubbed together, to remove extraneous coarse features from the paper. The electrode was polished until scratches on the surface were only those left by the polishing paper. The process was repeated using paper of successively finer grit: 280, 320 and finally 600 grit. Between polishing steps, the electrode was cleaned in an ultrasonic bath of concentrated alkali-detergent diluted with de-ionized water, followed by ultrasonic baths in de-ionized water, acetone, and finally methanol. The spherical electrode was vacuum degassed at 900 °C for 4 hours. The mounting cup and the screening electrode were polished and cleaned in the same manner as the spherical electrode, but they were not vacuum degassed. For ultra high vacuum quality considerations, both the mounting cup and the screening electrode should have been vacuum degassed. However this was not deemed necessary at the time of the tests since the objective was to determine the usefulness of the screening electrode.

2.3 INSTALLATION AND PREPARATORY PROCEDURES

The electrode/insulator assembly was cleaned with lint-free tissue and 2-propanol followed by a high-speed jet of CO_2 prior to installation in the vacuum chamber. The vacuum chamber with the electrode/insulator assembly was evacuated and baked at 250 °C for 48 hours. Afterwards, the vacuum level was typically below 5×10^{-9} Pa. Before inserting high voltage cables into insulators and receptacles, a thin layer of silicone "grease"

(approximately 0.2 cm thick) was applied to each cable termination to prevent air gaps in the interface between the plug and the insulator. Cable terminations were secured and maintained under compression using an aluminum flange that pressed the cable collar against the insulator vacuum flange, and pushed the cable into the insulator, providing an appropriate level of pressure at 1034 kPa (150 pounds per square inch). If this was not done correctly, voltage breakdown sometimes occurred, leaving a carbon track at the insulator-to-plug interface requiring costly cable repairs.

2.4 HIGH VOLTAGE GAS CONDITIONING

Key to the success of these high voltage tests was gas conditioning performed using krypton gas, a technique in which an inert gas was introduced into the vacuum chamber, with the cathode electrode biased at a voltage high enough to produce field emission [19]. Gas conditioning serves to eliminate field emitters from the cathode electrode through ion bombardment and resultant sputtering and ion implantation [20]. In addition, this technique is much more reliable than high voltage processing in vacuum and more importantly, it helps to limit damage to photogun components that often result from unregulated field emission [21]. To implement gas conditioning and prior to enabling high voltage, a constant flow of krypton was introduced into the vacuum chamber. A manual leak valve was set to provide a stable pressure of ~10^{-5} Pa at the turbo pump, which provided continuous pumping through a valve that was throttled closed, to reduce the pumping speed of the turbo pump. Pressure inside the vacuum chamber was ~ 10^{-3} Pa, based on conductance assumptions of the vacuum plumbing. The ion pumps on the vacuum chamber and pump cart were not energized. Three signals were monitored during gas conditioning: the vacuum inside the photogun (via residual gas analyzer and a cold-cathode vacuum gauge), field emission via Geiger counters mounted around the photogun vacuum chamber, and the high voltage power supply current. Some current draw was expected, as a result of non-problematic Ohmic current paths to ground, including the current across the high voltage power supply current measuring stack. Current draw above normal baseline values was an indication of field emission or breakdown. The voltage was initially set to 50 kV. If no field emission or excess current activity was observed, the voltage was increased in ~ 10 kV steps. If excess current activity was observed, the voltage increase was paused until field emission was extinguished. In some instances, voltage was increased regardless but ensuring the current would not exceed 100 μA above baseline. The high voltage power supply was operated in over-current trip mode, typically set to 400 μA. Gas conditioning was always implemented each time a new insulator/electrode configuration was tested.

Under successful conditions, an electrode-insulator configuration would reach 375 kV during krypton gas conditioning, and with negligible field emission, with Geiger counters registering less than 10 counts per second (with high voltage off, the Geiger counters registered less than 5 counts per second). The insulator-electrode configuration would then "soak" at 375 kV for several hours to determine the stability (robustness) of the configuration. It would take approximately 100 hours of high voltage processing to achieve this ideal situation. Afterwards, the voltage was decreased to zero, the krypton gas evacuated and once vacuum conditions were below 10^{-8} Pa, the voltage was slowly increased again to just 365 kV. By applying less voltage under vacuum conditioning (~ 10 kV), one avoids voltage-induced gas desorption, which can contribute to the formation of new field emitters, thereby necessitating further krypton gas conditioning [22]. In summary, the strategy of high voltage conditioning was as follows: an ideal electrode-insulator configuration would reach 375 kV via krypton gas conditioning, and then 365 kV under vacuum, for intended operation as a photogun at 350 kV.

3 RESULTS

3.1 R30 UNALTERED ALUMINA INSULATOR

Two R30 unaltered alumina insulators were tested (Figure 2a). During high voltage gas conditioning of the first sample, evidence of excess current was observed at 315 kV with no associated field emission activity (i.e., Geiger counters reading < 10 counts per second), indicating that the observed excess current was related to phenomena outside the vacuum environment. As high voltage processing continued, the pressure was observed to increase by more than two orders of magnitude for brief periods of time. The vacuum always recovered within seconds, making dubious the presence of a leak. The R30 unaltered alumina insulator reached 329 kV for a few minutes with no evidence of field emission before the high voltage power supply tripped off, indicating an over-current fault. Additional attempts to apply high voltage at previous levels were not successful. Upon removing the high voltage cable from the insulator, a carbon track was observed at the bottom of the insulator as shown in Figure 3a. Leak checking with helium indicated that the insulator wall was punctured. The tracking did not span the entire length of the insulator, but rather started at the high voltage end and terminated approximately 5 cm above, forming a crater at the puncture point.

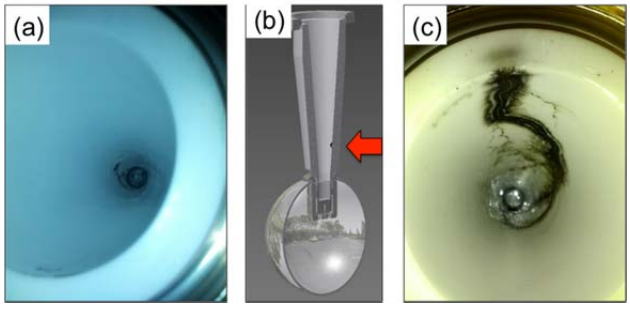

Figure 3. Damaged insulators. In (a) photograph of the first R30 unaltered alumina insulator, plug side, after failing at 329kV. The carbon track originates at the high voltage end and terminates ~ 5 cm above. Drawing of insulator and electrode (b) showing the approximate location of the puncture, coinciding with one end point of the carbon track, and (c) carbon tracking on the second R30 unaltered alumina insulator after failing at 300kV. The tracking spans the total length of the insulator. The color variations apparent in the two photographs was an inadvertent artifact of using different camera settings – the two insulators, before and after failure, were visually similar.

The second R30 unaltered alumina insulator was tested and field emission observed at 275 kV during high voltage gas conditioning. This field emission was successfully processed out and voltage was then slowly increased to 300 kV with no evidence of field emission or excess current. However, after a few minutes, the high voltage power supply tripped off, once again due to an over-current fault. Voltage could not be re-applied. Upon inspection, an obvious carbon trace was visible, spanning the entire length of the insulator from the high voltage end to ground (Figure 3c). There was no evidence of puncture in this instance.

3.2 R30 UNALTERED ALUMINA INSULATOR WITH SCREENING ELECTRODE

After the failure of the two R30 unaltered alumina insulators, a different electrode configuration was tested, composed of a new R30 unaltered alumina insulator, the spherical electrode, and a screening electrode that shields the vacuum-metal-insulator triple-point junction (Figure 2b). Field emission levels during high voltage gas conditioning were three orders of magnitude higher than those observed during tests of the R30 unaltered alumina insulators without the screening electrode. Despite tens of hours of high voltage krypton gas processing, field emission could not be eliminated. However, under high voltage conditions with krypton gas, the R30 unaltered alumina insulator with screening electrode reached 375 kV without breakdown, and sustained 370 kV for 4 hours. After pumping away the krypton gas, this configuration successfully soaked at 350 kV under ultrahigh vacuum conditions for 4 hours, albeit still exhibiting field emission three orders of magnitude higher than observed during tests of same type of insulator without the screening electrode. Given that the target voltage was reached, and in order to preserve the R30 insulator for future tests, the voltage was not increased further. The only difference between this successful result, and tests with the other two R30 unaltered alumina insulators that suffered breakdown at lower voltage, was the addition of the screening electrode.

3.3 R30 COATED ALUMINA INSULATOR

A fourth R30 unaltered alumina insulator was coated with a ZrO film on the vacuum side, to investigate if a slightly conductive coating would serve to dissipate surface charge buildup, and therefore increase the voltage holdoff [12, 13]. With the purpose of isolating the performance of the coating, the insulator was tested with the spherical electrode only as shown in Figure 2c. However for this test, the spherical electrode was polished further by hand starting with 320 grit paper and ending with 600 grit before transitioning to 9 μm diamond paste, then 6 μm and finally 1 μm. The electrode was chemically cleaned in ultra-sonic baths as described in section 2.2. Measured field emission levels were low and similar to those observed prior to the additional polishing procedure (Geiger counters reading < 10 counts per second), suggesting in retrospect, additional polishing with diamond paste was unnecessary.

High voltage conditioning with krypton gas proceeded similarly as with the previously tested R30 unaltered alumina insulators. At 336 kV, voltage induced gas desorption was observed without field emission [22]. At 340 kV, the high voltage power supply tripped off upon reaching the over current trip limit (400 μA). Upon recovering the voltage, field emission was observed at 200 kV, but processed out at 240 kV. At 300 kV, the high voltage power supply tripped off once more, but in this instance the vacuum level had increased two orders of magnitude. Upon inspection, a carbon track was observed, originating at the high voltage connection, and terminating about 2 cm below the ground end of the ceramic, with two punctures at the location shown in Figure 4. It is interesting to note that the punctures in the R30 ZrO coated insulator occurred near the ground end, while the puncture in the R30 unaltered alumina occurred at the opposite location near the high voltage end.

3.4 R28 DOPED ALUMINA INSULATOR

The R28 doped alumina insulator was tested using only the spherical electrode. This insulator had lower bulk resistivity compared to the R30 unaltered alumina insulators (Table 1). High voltage conditioning with krypton gas was performed following the same procedure as with the R30 insulators, observing typical field emission processing and voltage induced gas desorption. Excess current without associated field emission was never observed, indicating the problems associated with breakdown at the insulator/cable interface were not present. Despite being 7 cm shorter than the R30 insulators (Figure 2b), the R28 doped alumina insulator reached 360 kV for one hour without field emission, under krypton gas conditions. The voltage was not increased further with the intention to preserve the integrity of the insulator and high voltage cable plug. After gas conditioning, nominal ultrahigh vacuum conditions were re-established and the voltage was set to 350 kV for 5 hours on two separate occasions. Minimal field emission was observed in these two instances. The high voltage performance for all tested configurations along with insulator material properties are summarized in Table 1.

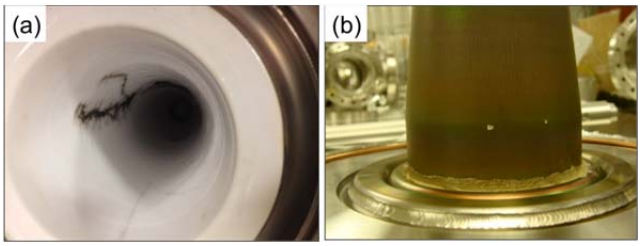

Figure 4. Photograph of the breakdown tracking on the plug side of the R30 ZrO coated insulator (a), and close-up photograph of the two punctures on the vacuum side of the ZrO coated R30 insulator (b). The punctures coincide with the location of the tracking termination position on the plug side.

3.5 ELECTROSTATIC MODELING

To estimate the field strength at the electrode and insulator surfaces, and to better appreciate the experimental results - especially those that involved breakdown - electrostatic field maps were generated using the field mapping software POISSON [23]. Although this software is more ideally suited for configurations that possess cylindrical symmetry, it is free and widely used. The field maps for three configurations are shown in Figure 5.

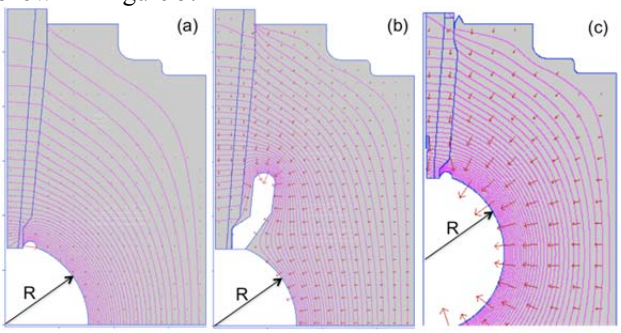

Figure 5. Electrostatic modeling results at 350kV for (a) R30 unaltered alumina insulator, (b) R30 unaltered alumina insulator with screening electrode, and (c) R28 doped alumina insulator. The equipotential lines are shown in pink. Red arrows represent the electric field. R=7.62 cm is the test electrode radius, which is the same in all three cases shown. The vertical axis represents the axis of symmetry of the insulator and high voltage plug, and the horizontal axis points in the direction of the beam delivery, along the center bore of the photogun.

Cylindrical symmetry was defined with respect to the axis of the insulator with Neumann boundary conditions on the left, top and bottom, while the vacuum chamber dimensions define Dirichlet boundary conditions on the right. The center conductor of the high voltage cable plug was modeled as a vertical metal rod with 0.5 cm diameter. The vulcanized rubber between the center conductor and the insulator wall was modeled as a material with dielectric constant $\varepsilon_1/\varepsilon_0$ of 2.37. The dielectric constant for each insulator was set according to the parameters listed in Table I. Our electrostatic modeling is similar to that in [24] of an inverted geometry ceramic insulator utilizing the finite element method at 100 kV but details are not provided about the ceramic or the cable plug dielectric constant and resistivity.

At 350 kV the maximum field strength on the spherical test electrode was ~ 7 MV/m for each configuration, whereas the field strength at the crown of the screening electrode was 12 MV/m (Figure 5b). The comparatively higher field strength at the screening electrode surface likely explains why field emission was more prominent for this test configuration. Optimization of the shape and size of the screening electrode, in combination with additional polishing steps, would serve to reduce the field strength and minimize field emission. These steps will be taken in the future, however the focus of this work was to evaluate breakdown at the interface between the high voltage cable plug and the insulator.

It is prudent to engineer high voltage insulator/electrode configurations to obtain a uniform potential gradient across the length of the insulator [25]. For our apparatus, this is represented by the black straight line in Figure 6, labeled "ideal potential".

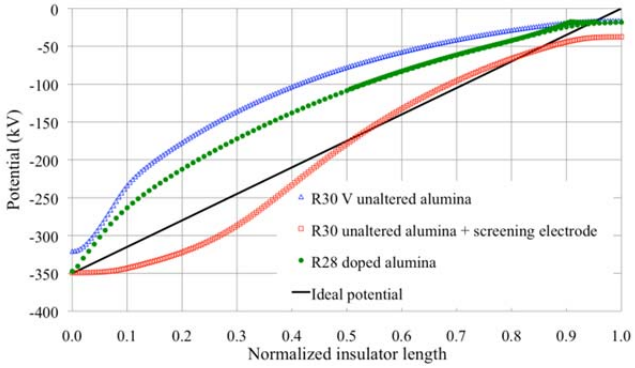

Figure 6. The potential along the insulator (normalized to 1) for each insulator/electrode configuration. The potential for the R30 unaltered alumina insulator with screening electrode exhibits a potential gradient closest to ideal.

Deviations from this linear potential, and with a steeper slope, represent conditions that provide higher field strengths that can lead to breakdown [25]. Of the three test configurations, the potential along the length of the R30 unaltered insulator varied most sharply compared to the ideal potential, especially near the high voltage end. This is consistent with our test results that showed the R30 unaltered insulator exhibited the worst high voltage performance. Furthermore, the largest variation in electric potential (i.e., the highest field strength) was in the vicinity of the origin of the carbon tracks and puncture. The screening electrode configuration provided the closest approximation to ideal,

Table 1. Material properties for each insulator/electrode test configuration and corresponding high voltage performance. The R30 insulators were composed of unaltered 97.7% alumina, while the R28 doped insulator was 94.7% alumina. The manufacturer provided the alumina concentration for each insulator type and corresponding transversal resistivity and dielectric constant. All test were performed using the same spherical test electrode.

Insulator type	Length (cm)	Transversal resistivity (Ohm-cm)	Dielectric constant $\varepsilon_1/\varepsilon_0$	Maximum voltage (kV)	Performance
R30 sample 1	20	$5.0\text{x}10^{15}$	9.1	329	Breakdown and puncture near high voltage end
R30 sample 2	20	$5.0\text{x}10^{15}$	9.1	300	Breakdown
R30 with additional screening electrode	20	$5.0\text{x}10^{15}$	9.1	375	370 kV with krypton 4-hr soak, 350 kV in vacuum 4-hr soak. Significant field emission in both cases
R30 ZrO-coated	20	$5.0\text{x}10^{15}$	9.1	340	Breakdown and puncture near ground end
R28 doped	13	$7.4\text{x}10^{11}$	8.4	360	360 kV with krypton 1-hr soak, 350kV in vacuum 5-hr soak, 2 times Minimal field emission in both cases

and the R28 doped insulator exhibited a potential gradient somewhat better than the R30 unaltered insulator configuration. These field mapping results are consistent with high voltage test results, namely, the two configurations that exhibit the most uniform potential drop across the insulator, also performed the best, each reaching the 350 kV goal.

Further discussion is warranted for the shorter R28 doped insulator. It must be noted that POISSON does not accommodate modeling of insulators with varying bulk or surface resistivity, and therefore the improved linearization of the potential gradient across the insulator length was simply a result of the test electrode being closer to ground. However, separate simulations of a larger conical-shaped doped insulator utilizing finite-element-method software show that a decreasing bulk resistivity serves to linearize the potential gradient across the insulator [26]. Bulk resistivity provides another potential benefit, namely, it serves to dissipate trapped charge that may originate from field-emitted electrons striking the insulator surface, from internal ionization at the insulator-vacuum interface and other processes [12-16]. It is therefore difficult to infer if the better performance of the short R28 doped alumina insulator stems from simple geometrical conditions or from its lower bulk resistivity. This will be discussed in more detail below.

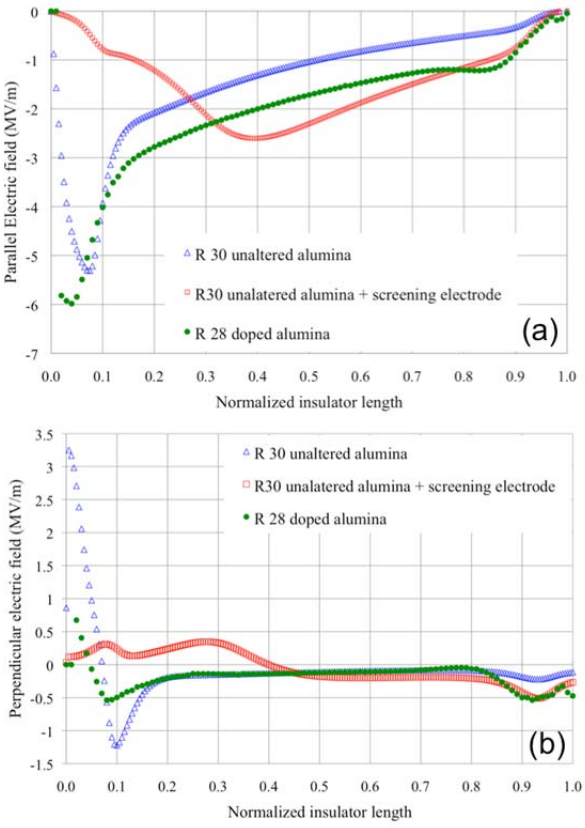

Figure 7. Electric field strength along the normalized insulator length for each insulator/electrode configuration. In (a) field strength parallel to the insulator surface, and (b) field strength perpendicular to the insulator surface.

The electrostatic field maps were assessed in further detail by plotting the field strength along the length of the insulator, both parallel and perpendicular to the insulator surface. An ideal insulator/electrode configuration exhibits some non-zero, but modest, field strength parallel to the surface of the insulator wall, and zero field strength perpendicular to the surface of the insulator wall [27]. Figure 7 shows field strengths across the insulator length, obtained from the POISSON field maps shown in Figure 5. These graphs indicate that the R30 unaltered alumina insulator with screening electrode approaches the ideal insulator/electrode configuration, exhibiting the smallest field strength parallel to the insulator surface (< 3 MV/m), and with nearly zero field strength perpendicular to the insulator surface (< 0.5 MV/m). In contrast, the R30 unaltered alumina insulator, without screening electrode, exhibits very high field strength near the high voltage end, both parallel and perpendicular to the insulator surface, 5.3 and 3.2 MV/m respectively. As stated previously, these results are compatible with our test results; namely, the R30 unaltered alumina insulator with screening electrode performed the best, while the R30 unaltered alumina insulator without screening electrode performed worst.

Interpreting the field strength results for the short R28 doped insulator is not as straightforward. Of the three configurations, this insulator exhibits the highest field strength value parallel to the insulator surface, 6 MV/m, near the high voltage connection. However, field strength values perpendicular to the insulator surface are small, < 1 MV/m. It is possible that the most critical parameter in determining insulator performance is the perpendicular component of the field strength, and this value should be small, as was the case for the R28 doped insulator. Or, as mentioned previously, the benefits of bulk and surface resistivity, are simply not manifest in the POISSON results, due to the software's limitations, and therefore the high field strength values parallel to the insulator surface might not accurately represent the conditions of the actual R28 doped insulator nor those of the R30 unaltered coated with ZrO.

4 OBSERVATIONS AND ANALYSIS

There is a vast literature describing high voltage studies aimed at developing reliable methods to bias electrodes at high voltages and at high field strengths [12-17, 24-30]. This section aims to put our work into context of similar work, related to insulators having different levels of bulk resistivity/conductivity, the benefits of using screening electrodes that shield triple-point junctions, and surface coatings.

Despite being 7 cm shorter, the R28 doped alumina insulator reached 365kV without failure, while two R30 unaltered alumina insulators suffered breakdown at ~ 300 kV. As mentioned above, the modeling software POISSON predicts a more uniform potential gradient across the insulator length due to simple geometrical conditions. But it is also plausible that benefits arise due to bulk resistivity that

serves to dissipate of trapped charges, as reported for doped alumina insulators with various concentrations of magnesium, titanium and chromium – which intrinsically lower the resistivity in otherwise unaltered alumina [12-16]. This was the motivation behind the test of the R28 doped alumina insulator whose transverse bulk resistivity is four orders of magnitude lower than the R30 unaltered alumina insulator (Table I). It was not clear from the electrostatic modeling which factors contribute to improved high voltage performance of the R28 doped insulator, namely: a) the potential being more linear due to geometrical reasons, b) the material having some degree of conductivity that contributes to dissipation of trapped charges, and/or c) the field strength perpendicular to the insulator surface near the triple junction was much smaller compared to the R30 unaltered insulator. Perhaps benefits arise from a combination of all three factors [16].

The benefit of the triple-point screening electrode was readily apparent, in that the screening electrode enabled the R30 unaltered alumina insulator to reach 375 kV without breakdown, whereas the same type of insulator failed repeatedly at ~ 300kV without the screening electrode. Our simulation results using POISSON indicated that the screening electrode provided the smallest parallel and perpendicular field strengths on the insulator surface, and this is consistent with observations in [28,29] that small electric field strengths at the cathode triple-junction significantly increase the voltage holdoff, since pre-breakdown current can be initiated by field-emitted electrons from the triple-junction for sufficiently high fields [16]. It is interesting to note that the experimental setup in [30] is similar to the inverted conical ceramic insulator, in the sense that there was vacuum on one surface of the insulator, and air on the other surface. Increased pulsed flashover voltage holdoff is also reported in [17] when a triple-junction screening cathode is utilized instead of a plate cathode. It is worth mentioning that the exposed length of the R30 insulator with screening electrode was comparable to that of the shorter R28 insulator, and that the screening electrode configuration effectively creates recessed electrode geometry near the insulator, for which the parallel field is greatly reduced near the triple-junction.

It is difficult to conclude if the improved high voltage performance of the R30 unaltered alumina insulator with screening electrode was due to a more "linearized" potential gradient across the insulator length, or because the screening electrode served to suppress conditions for pre-breakdown current at the triple point junction, or a combination of both. However in [12] the apparent surface charge becomes more uniformly distributed when the equivalent surface potential varies more linearly along the insulator, a characteristic we observe in Figure 6 for the R30 unaltered alumina insulator with screening electrode configuration.

Our observations regarding the benefit of linear potential across 20 cm long insulators are in contradiction with those by Pillai and Hackam [27] where the dc flashover voltage was higher for 0.2 cm long conical insulator (negative angle) with non-linear potential gradient, than for a cylindrical insulator with linear potential. Since the electrode shape, size and bulk resistivity influence the linearity of potential, it is difficult to directly compare our results with those in [27]. However, our observations are consistent regarding field enhancement when the narrow end (negative angle in [27]) of the insulator is at the cathode, favoring conditions for breakdown.

Although the performance of the ZrO-coated R30 insulator was not as good as the R28 doped alumina insulator or the R30 unaltered alumina with screening electrode, the coating improved the holdoff voltage from ~ 300 kV to 340 kV. This result is consistent with experiments performed in [12-13] using small solid insulators placed between two electrodes in vacuum, which show that oxide coatings indeed increase the holdoff voltage. A surface layer on the insulator with lower resistivity and lower secondary electron yield improves the voltage holdoff by reducing positive charge buildup at the cathode that suppresses the pre-breakdown current process [12]. In our experiments, the outer surface of the 20 cm long R30 inverted-geometry ceramic insulator was in vacuum, while the inner surface was in contact with the high voltage cable plug that included a thin layer of silicon grease, to minimize trapped air at the insulator/cable interface. Since breakdown occurred at this interface, a resistive coating similar to that tested in [12] might be beneficial if applied to both insulator surfaces. More tests are planned with precise tuning of the coating resistivity and secondary electron yield. If breakdown was due solely to surface effects, the low resistivity ZrO coated R30 insulator would have performed better, but as reported in [15] and [16], dopant species and micro-structural parameters determine the capability to trap, and to dissipate charges in the bulk of the ceramic insulator, supporting our observations of the better performance of the R28 with bulk low resistivity, compared to the ZrO coated R30 insulator with low surface resistivity.

The ZrO-coated R30 insulator suffered a puncture near the ground-end of the insulator, rather than near the high voltage side, as was the case for the R30 unaltered alumina insulator sample 1. For R30 unaltered alumina insulator sample 2, voltage breakdown caused a track on the cable plug/ceramic interface spanning the entire length from cathode to ground (Figure 3c), but no puncture. It appears as if the current path in sample 1 started near the cathode electrode, continued through the silicon grease between plug and ceramic, and then through the ceramic wall into the vacuum and terminated at the ceramic ground end (Figures 2a and 3b). A similar path was observed inside the ZrO-coated R30 insulator but the puncture was near the ground end (Figure 4). Additional simulations, not included in this paper, show that if an air gap or small volume is placed in the plug-ceramic interface, the field strength perpendicular to the insulator wall is significantly enhanced at that location. It is plausible that the results were driven by the cable plug installation procedure, but it is difficult to draw a conclusion due to lack of statistics, i.e. breakdown was observed in three out of three

tests with identical ceramic-electrode configuration, with two of them showing punctures. Although the difference in the maximum voltage achieved by the two R30 unaltered alumina insulators without screening electrode is about 10%, it seems that this configuration experiences breakdown near 300kV. However, this observation cannot be asserted due to the limited number of tests, which are restricted by the cost and manufacturing time of insulator samples.

5 FUTURE WORK

Based on the very favorable results using the short R28 doped insulator, longer R30 doped insulators will be purchased, with bulk resistivity comparable to that of the tested insulator. Evaluation of this new insulator will help de-couple the beneficial effect of the screening electrode from the beneficial effect of ceramic insulators having bulk resistivity. Electrostatic simulations will be performed to optimize the shape and size of a new screening electrode, with the goal to minimize field enhancement while still grading the potential across the length of the insulator and providing screening of the triple-junction. The optimized screening electrodes will be vacuum degassed in future tests to conform with our standard ultra high vacuum techniques. Electrostatic simulations will be performed using 3D compatible software that can account for material properties such as bulk resistivity and secondary electron yield.

6 CONCLUSION

Three types of inverted-geometry ceramic insulators, and two electrode configurations, were tested inside a photogun vacuum chamber with the purpose of developing an inverted-ceramic/electrode geometry capable of reaching 375 kV, without electrical breakdown for nominal operation at 350 kV. Two configurations were found to improve the voltage holdoff capabilities of tested insulators: an alumina insulator 13 cm long with commercial denomination R28 and doped with proprietary formulation for low bulk resistivity, and a 20 cm long unaltered alumina insulator with commercial denomination R30 with an additional screening electrode. Both of these configurations reached the stated goal of sustained operation at 350 kV. Our experimental results and electrostatic modeling analyses indicate that the holdoff voltage between the photogun insulator and the commercial high voltage cable connecting to the high voltage dc power supply, was effected by a combination of factors including the potential gradient across the length of the insulator, the electrode/insulator geometry, and the insulator bulk resistivity. These parameters likely influence the level of trapped charge that can accumulate on the insulator surfaces, and the electric field strength at the triple-junction, however, the contribution of each factor, as it relates to the ultimate performance of each insulator/electrode configuration, was difficult to decouple.

ACKNOWLEDGMENT

Authored by Jefferson Science Associates, LLC under U.S. DOE Contract No. DE-AC05-06OR23177. The U.S. Government retains a non-exclusive, paid-up, irrevocable, world-wide license to publish or reproduce this manuscript for U.S. Government purposes. This material is based upon work supported by the U.S. Department of Energy, Office of Science, Office of Nuclear Physics under contract DE-AC05-06OR23177. The authors would like to thank F. Hannon, D. Bullard, J. Clark, Y. Wang, M. Stutzman, P. Adderley, and W. Moore for their contributions to this work; and to J. Benesch for useful comments.

REFERENCES

[1] W. Anders, I. Bazarov, L. Cultrera, D. Dimitrov, D. H. Dowell, B. Dunham, J. W. Lewellen, A. Nuewmann, M. Poelker, T. Rao, S. Schreiber, J. Smedley and T. Tsang, edited by T. Rao and D. H. Dowell, *An engineering guide to photoinjectors*, Ch 8. (ISBN-13, 978-1481943222, ISBN-10:1481943227, 2013).

[2] J. Grames, P. Adderley, J. Brittian, J. Clark, J. Hansknecth, D. Machie, M.Poelker, M. L. Stutzman, R. Suleiman and K. Surles-Law, "Lifetime measurements of high polarization strained-superlattice gallium arsenide at beam current >1 milliamp using a new 100 kV load lock photogun", Particle Accelerator Conf., Albuquerque, NM, USA, pp. 3130-3132, 2007.

[3] J. E. Clendenin, T. Kotseroglou, G. A. Mullhollan, D. T. Palmer, and J. F. Schmerge, "Generation of low emittance beams using III-V semiconductor photocathodes in an rf gun", SLAC-PUB-8355, LCLS-TN-00-02, 2000, 2nd ICFA Advanced Accelerator Workshop on the Physics of High Brightness Beams, UCLA Faculty Center, Los Angeles, CA, USA, 1999.

[4] P. A. Adderley, J. Clark, J. Grames, J. Hanskecht, K. Surles-Law, D. Machie, M. Poelker, M. L. Stutzman, and R. Suleiman, "Load-locked dc high voltage GaAs photogun with an inverted-geometry ceramic insulator", Phys. Rev. ST Accel. Beams 13 010101, 2010.

[5] D. Engwall, C. Bohn, L. Cardman, B. Dunham, D. Kehne, R. Legg, H. Liu, M. Shinn, and C. Sinclair, "A high-dc-voltage GaAs photoemission gun: transverse emittance and momentum spread measurements", Particle Accelerator Conf., Vancouver, BC, Canada, edited by M. Comyn, M. K. Craddock, M. Reiser, and J. Thomson, pp. 1-3, 1997.

[6] N.Nishimori, R. Nagai, S. Matsuba, R.Hajima, M.Yamamoto, Y.Honda, and T. Miyajima, "Experimental investigation of an optimum configuration for a high-voltage photoemission gun for operation at >500 kV", Phys. Rev. ST Accel. Beams, Vol. 17, 053401 (2014).

[7] J. Maxon, I. Bazarov, B. dunham, J. Dobbins, X.Liu, and K. Smolenski, "Design, conditioning, and performance of a high voltage, high brightness dc photoelectron gun with variable gap", Rev. Sci, Instrum. Vol. 85, 093306, 2014.

[8] M. Breidenbach, M. Foss, J. Hodgson, A. Kulikov, A. Odian, G. Putallaz, H. Rogers, R. Schindler, K. Skarpaas, and M. Zolotorev, "An inverted-geometry, high voltage polarized electron gun with UHV load lock", Nucl. Instr. and Meth., Phys. Res. A, Vol. 350, pp. 1-7, 1994.

[9] W. von Drachenfels, F. Frommberger, M. Gowin, W. Hillert, M. Hoffmann, and B. Neff, "The polarized source at ELSA", [SPIN 2002: 15th Int'l. Spin Physics Symposium and Workshop on Polarized Electron Sources and Polarimeters, edited by Y. I. Makdisi, A. U. Luccion, and W. W. MacKay, American Institute of Physics, pp. 1053-1057, 2003.

[10] P. Adderley, J. Clark, J. Grames, J. Hansknecht, M. Poelker, M. Stutzman, R. Suleiman, K. Surles-Law, J. McCarter, and M. BastaniNejad, "CEBAF 200kV inverted electron gun", [Proceedings of the 2011 Particle Accelerator Conference, New York, NY, USA, pp. 1501-1503, 2011.

[11] Md Abdullah A. Mamun, Abdelmageed A. Elmustafa, Marcy. L. Stuttzman, Phillip A. Adderley, and Mathhew Poelker, "Effect of heat treatments and coatings on the outgassing rate of stainless steel chambers", J. Vac. Sci. Technol. A., Vol. 32, 021604, 2014.

[12] N. C. Jaitly and T. S. Sudarshan, "dc surface flashover mechanism along solids in vacuum based on a collision ionization model", J. Appl. Phys, Vol. 64, pp. 3411-3418, 1988.

[13] L. L. Hatfield, E. R. Boerwinkle, G. R. Leiker, H. Kromholz, R. Korzekwa, M. Lehr, and M. Kristiansen, "Methods of increasing the surface flashover potential in vacuum", IEEE Trans. Electr. Insul., Vol 24, pp. 985-990, 1989.

[14] Y. J. Lei, B. H. Tang, X. J. Huang, Y. Huang, X. F. You, M. Zeng, "Effects of bulk doping on surface insulating performance of alumina ceramic in vacuum", IEEE Trans. Dielectr. Electr. Insul., Vol., 18, pp. 2103-07, 2011.
[15] J. Liebault, J. Vallayer, D. Goeuriot, D. Treheux, and F. Thevenot, "How the trapping of charges can explain the dielectric breakdown performance of alumina ceramics", J. European Ceramic Soc., Vol. 21, 389-397, 2001.
[16] H. C. Miller, "The effect of doping on the voltage holdoff performance of alumina insulators in vacuum", IEEE Trans. Electr. Insul. Vol. 20 No. 3, pp. 505-509, 1985.
[17] C. Yanlin, X. Wei, and L. Ming, "Influence of electrode geometry on pulsed surface flashover of the alumina insulator in vacuum", IEEE Trans. Plasma Scie., Vol., 41, No. 8, pp. 2123-2127, 2013.
[18] J. Francis, SLAC Procedural Note FP-238-042-94 (1991).
[19] R. L. Latham, *High Voltage Vacuum Insulation*, Academic Press, London, 1995.
[20] M. BastaniNejad, A. A. Elmustafa, E. Forman, J. Clark, S. Covert, J. Grames, J. Hansknecht, C. Hernandez-Garcia, M. Poelker and R. Suleiman, "Improving the performance of stainless-steel DC high voltage photoelectron gun cathode electrodes via gas conditioning with helium or krypton", Nucl. Instr. and Meth. in Phys. Res. A, Vol. 762, pp. 135–141, 2014.
[21] C. Hernandez-Garcia, S. V. Benson, G. Biallas, D. Bullard, P. Evtushenko, K. Jordan, M. Klopf, D. Sexton, C. Tennant, R. Walker, and G. Williams, "dc high voltage conditioning of photoemission guns at Jefferson Lab FEL", AIP Conf. Proc. 1149, pp. 1071-1076, 2009.
[22] W. T. Diamond, "New perspectives in vacuum high voltage insulation. II. Gas desorption", J. Vac. Sci, Technol. A, Vol. 16, No. 2, pp. 720-735, 1998.
[23] K. Halbach, "LANL SUPERFISH", Lawrence Livermore National Laboratory Technical Report No. UCRL-17436, 1967.
[24] H. Watanabe, N. Yoshimura, S. Katoh, and N. Kobayashi, "Microdischarges on an electron gun under high vacuum", J. Vac. Sci. Technol, A, Vol. 5, No. 1, 1987, pp 92-97, 1987.
[25] A. S. Pillai and R. Hackam, "Modification of electric field at the solid insulator-vacuum interface arising from surface charges on the solid insulator", J. Appl. Phys, Vol. 54, pp. 1302-1313, 1983.
[26] F.E. Hannon, P. Evtushenko, and C. Hernandez-Garcia, "Electrostatic modeling of the Jefferson Laboratory inverted ceramic gun", Int'l. Particle Accelerator Conf., Kyoto, Japan, pp. 383-385, 2010].
[27] A. S. Pillai and R. Hackam, "Surface flashover of conical insulators in vacuum", J. Appl. Phys., Vol. 56, pp. 1374-1381, 1984.
[28] H. C. Miller, "Surface Flashover of Insulators", IEEE Trans. Electr. Insul., Vol. 24, No. 5, 1989, pp. 765-786, 1989.
[29] A. S. Pillai and R. Hackam, "Influence of metalinsulator junction on surface flashover in vacuum", J. Appl. Phys., Vol. 61, pp. 4992-4999, 1987.
[30] J. P. Brainard and D. Jensen, "Electron avalanche and surface charging on alumina insulators during pulsed high voltage stress", J. Appl. Phys., 45, (1974), pp. 3260-3265, 1974.

Carlos Hernandez-Garcia (M'14) Received the Ph.D. degree in physics from Vanderbilt University in 2001. Shortly afterwards he started work at Jefferson Lab with the Free Electron Laser project, where in 2004 was appointed photo-injector group manager. In 2012 he moved to the Accelerator Division where he has been working on compact dc photoemission guns based on inverted geometry insulators and multi-alkali photocathodes. Since 2010 Dr. Hernandez-Garcia has served as facilitator between the Mexican Physical Society and various USA National Laboratories to train a new generation of Mexican students in accelerator physics. His professional career has been focused on R&D of high brightness and high voltage dc photoemission electron guns for accelerator based applications. He is now on sabbatical leave at Deutsches Elektronen-Synchrotron (DESY) Photo Injector Test Facility, studying electron emission from Telluride photocathodes in radio-frequency electron guns.

Bernard Matthew Poelker received the B.S. degree in engineering physics from the University of Illinois, Urbana-Champaign in 1983, and the M.S. and Ph.D. degrees from Northwestern University in 1988 and 1992, respectively. Following a post-doctoral appointment at Argonne National Laboratory, he joined Jefferson Lab in 1994, to help develop reliable sources of spin polarized electrons for use at the Continuous Electron Beam Accelerator Facility, a nuclear physics research facility. He now heads the Center for Injectors and Sources, where research topics include dc high voltage photoguns, ultrahigh vacuum, photocathodes and drive lasers. He and other members of the group have published approximately 20 papers on these topics. He was recently awarded the Ernest O. Lawrence award by the U.S. Department of Energy, for efforts that have multiplied the effectiveness of accelerators in providing the beams of electrons that experimenters use for probing and elucidating the quark structure of the atom's nucleus.

John C. Hansknecht graduated from the Naval Nuclear Power School in 1984. He received his A.S. degree from Thomas Nelson Community College in 2000. He started work at Jefferson Lab in 1988 with the Cryogenics group of the Engineering Division. He moved to the Accelerator Division in 1995, where he builds lasers, electronic control circuitry, and high voltage systems associated with the spin polarized electron source used at the nuclear research facility known as the Continuous Electron Beam Accelerator Facility, operated by the Department of Energy. In 2007, he started Laser Safety Systems, a business that specializes in interlock circuitry to mitigate laser hazard.